

# Microscopic investigation of magneto-optical activity in the ternary compounds PtMnSb, PdMnSb, NiMnSb, and PtMnSn

Yu. A. Uspenskiĭ

*I. E. Tamm Theoretical Department, P. N. Lebedev Physics Institute, Russian Academy of Sciences, 117924 Moscow, Russia*

É. T. Kulatov

*Institute of General Physics, Russian Academy of Sciences, 117942 Moscow, Russia*

S. V. Khalilov

*Department of Theoretical Solid State Physics, University of Duisburg, Germany*

(Submitted 30 December 1994)

Zh. Éksp. Teor. Fiz. **107**, 1708–1721 (May 1995)

The shaping of the magneto-optical spectrum of the compounds PtMnSb, PdMnSb, NiMnSb, and PtMnSn with a  $C1_b$  structure has been studied in detail. Microscopic calculations correctly reproduce the basic features of the experimental magneto-optical spectra of this group of compounds: the shape of the curves, the positions of the extrema, the relatively small magnitude of the polar Kerr rotation in PdMnSb, NiMnSb, and PtMnSn, and the large magneto-optical resonance with an energy of 1.7 eV in PtMnSb. It has been shown that the magneto-optical resonance in PtMnSb is caused mainly by excited electrons with spin down and is closely related to the presence of an energy gap at the Fermi level. An important effect associated with the influence of the diagonal components of the dielectric tensor on the level of magneto-optical activity has been discovered. © 1995 American Institute of Physics.

## 1. INTRODUCTION

The investigation of compounds with high magneto-optical activity is of great importance both for applications (the search for materials for magneto-optical disks) and for achieving a deeper understanding of the electronic structure and magnetic properties of solids. The compound PtMnSb has the greatest known rotation of the plane of polarization under the polar Kerr effect at room temperature,  $\theta_K = -2^\circ$ , which is observed over a narrow energy range near  $\hbar\omega = 1.7$  eV.<sup>1–4</sup> Similar spikes of  $\theta_K(\omega)$  (magneto-optical resonances) are characteristic of many materials with high magneto-optical activity. Their origin remains largely unclear, and even the question of whether they are caused by spikes in the off-diagonal components of the dielectric tensor or by the behavior of the diagonal components continues to be debated in the literature.<sup>5–7</sup> One popular explanation<sup>8</sup> relates the magneto-optical resonance in PtMnSb to the unusual electronic structure of this compound, which is a metal for electrons with spin up (in the direction of the magnetic moment) and a semiconductor for electrons with spin down. Such a half-metallic ferromagnetic state is also characteristic of the isotopic compounds NiMnSb and PdMnSb (Ref. 8).<sup>1</sup> However, the Kerr rotation does not exceed  $0.3^\circ$  in these two compounds or in PtMnSn, which all have the same  $C1_b$  crystal structure as PtMnSb and a similar chemical composition.<sup>1</sup> These facts, as well as the microscopic mechanism shaping the magneto-optical resonance in PtMnSb and the roles of the different atoms in this process, have not yet been satisfactorily explained.

*Ab initio* calculations of the magneto-optical spectra of ferromagnetic compounds make it possible to study these

questions in great detail. Such calculations have already been successfully employed in the analysis of the magneto-optical spectra of ferromagnetic  $3d$  metals.<sup>9</sup> Such an analysis is performed in the present work for PtMnSb, PdMnSb, NiMnSb, and PtMnSn. The large differences between the magneto-optical spectra of these substances make it possible to test the quality of the microscopic calculations and to thoroughly investigate the factors determining the magnitude of the magneto-optical effects in this group of compounds. Special attention is devoted to studying the magneto-optical resonance in PtMnSb and its relationship to features of the electronic structure of this compound. For this purpose we performed a large number of numerical experiments, which yielded information that is virtually inaccessible to purely experimental investigative methods.

## 2. MICROSCOPIC CALCULATION OF MAGNETO-OPTICAL EFFECTS

The rotation of the plane of polarization and the ellipticity observed under the polar Kerr effect  $\theta_K(\omega)$  and  $\epsilon_K(\omega)$  are related to the dielectric tensor  $\epsilon_{\alpha\beta}(\omega) = \epsilon_{1,\alpha\beta}(\omega) + i\epsilon_{2,\alpha\beta}(\omega)$  by

$$\theta_K(\omega) + i\epsilon_K(\omega) = \frac{\epsilon_{xy}(\omega)}{(1 - \epsilon_{xx}(\omega))\sqrt{\epsilon_{xx}(\omega)}}, \quad (1)$$

which holds true for cubic crystals with a direction of the magnetic moment  $\mathbf{M} \parallel [001]$ . In this configuration the absorption of light is determined by the components  $\epsilon_{2,xx}(\omega)$  and  $\epsilon_{1,xy}(\omega)$ . If the absorptive part of the dielectric tensor

$\varepsilon_{\alpha\beta}^{\text{abs}}(\omega)$  is known over a broad range of energies, the dispersive part of the tensor can be found using the Kramers–Kronig relations:

$$\varepsilon_{1,xx}(\omega) = 1 + \frac{2}{\pi} P \int d\omega' \frac{\omega' \varepsilon_{2,xx}(\omega')}{\omega'^2 - \omega^2}, \quad (2)$$

$$\varepsilon_{2,xy}(\omega) = -\frac{2}{\pi} P \int d\omega' \frac{\omega' \varepsilon_{1,xy}(\omega')}{\omega'^2 - \omega^2} \quad (3)$$

In the widely employed random-phase approximation neglecting local field effects, the interband part of  $\varepsilon_{\alpha\beta}^{\text{abs}}(\omega)$  is given by

$$\varepsilon_{\alpha\beta}^{\text{inter,abs}}(\omega) = \frac{4\pi^2 e^2 \hbar^2}{m^2 \omega^2 \Omega} \sum_{i,f} \int d\mathbf{k} p_{\alpha}^{i,f}(\mathbf{k}) p_{\beta}^{f,i}(\mathbf{k}) \delta(E_{f_i}(\mathbf{k}) - \hbar\omega) [\theta(E_{f_i}(\mathbf{k})) - \theta(E_{i_i}(\mathbf{k}))], \quad (4)$$

where  $E_{f_i}(\mathbf{k}) = E_f(\mathbf{k}) - E_i(\mathbf{k})$  and the transition matrix element between the initial ( $i$ ) and final ( $f$ ) states equals  $p_{\beta}^{f,i}(\mathbf{k}) = \langle f | \mathbf{k} | \hbar \nabla_{\beta} | i \rangle$ . The intraband part of the diagonal components of  $\varepsilon_{\alpha\beta}(\omega)$  is generally described using the Drude formula:

$$\varepsilon_{xx}^{\text{intra}}(\omega) = 1 - \frac{\tilde{\omega}_p^2}{\omega(\omega + i\gamma)}, \quad (5)$$

$$\tilde{\omega}_p^2 = \frac{4\pi e^2 m}{\hbar \Omega} \sum_i \int d\mathbf{k} \delta(E_i(\mathbf{k}) - E_F) (\nabla_{k_x} E_i(\mathbf{k}))^2. \quad (6)$$

As for the intraband contribution to the off-diagonal components of the dielectric tensor, the corresponding microscopic expression has not yet been obtained, despite repeated discussions of this question (see, for example, Ref. 5).

Expression (4) is widely used in numerical calculations of  $\varepsilon_{\alpha\beta}(\omega)$ . It does not, however, make it possible to analytically trace the dependence of  $\varepsilon_{\alpha\beta}(\omega)$  on the main factors for magneto-optics, viz., spin polarization and spin–orbit coupling. The expressions derived from (4) to lowest order in the spin–orbit coupling are most suitable for this purpose. In this approximation  $\varepsilon_{2,xx}(\omega)$  is simply the sum of the contributions from the excitations of electrons with spin up and with spin down. The expression for  $\varepsilon_{1,xy}(\omega)$  is more complicated:<sup>10</sup>

$$\varepsilon_{1,xy}(\omega) = \frac{4\pi^2 e^2 \hbar^2}{m^2 \omega^2 \Omega} \sum_{i,f \neq i} \int d\mathbf{k} \{ [H_{\text{SO},z}^{il}(\mathbf{k}) p_x^{i,f}(\mathbf{k}) p_y^{f,i}(\mathbf{k}) / E_{f_i}(\mathbf{k}) + H_{\text{SO},z}^{fi}(\mathbf{k}) p_x^{f,i}(\mathbf{k}) p_y^{i,f}(\mathbf{k}) / E_{f_i}(\mathbf{k}) - [x \leftrightarrow y]] [\theta(E_{f_i}(\mathbf{k})) - \theta(E_{i_i}(\mathbf{k}))] \times \delta(E_{f_i}(\mathbf{k}) - \hbar\omega), \quad (7)$$

where

$$H_{\text{SO},z}^{i,l} = \langle i | \mathbf{k} | \hat{\sigma}_z [ \nabla_x V(\mathbf{r}) \nabla_y - \nabla_y V(\mathbf{r}) \nabla_x ] | l \rangle \hbar^2 / 4m^2 c^2$$

and  $V(\mathbf{r})$  is the crystal potential. Since the Pauli matrix  $\hat{\sigma}_z$  is diagonal in the spin indices, expression (7) describes the difference between the contributions from the excitations of electrons with spin up and spin down. The presence of ma-

trix elements from three operators, viz.,  $\hat{p}_x$ ,  $\hat{p}_y$ , and  $\hat{H}_{\text{SO}}$ , in (7) indicates that the behavior of the wave functions within a particular atomic cell influences  $\varepsilon_{1,xy}(\omega)$  in three ways: through the  $x$  and  $y$  components of the dipole moments created by the particular atom and through the effective spin–orbit coupling at the particular lattice site. In addition, due to the presence of the spin operator  $\hat{\sigma}_z$  in  $\hat{H}_{\text{SO},z}$ , the contribution of a given lattice site to the effective spin–orbit coupling is strictly related to the spin polarization at that site. The functional relations noted were used in the present work to numerically investigate the shaping of the magneto-optical spectra of compounds and to specify the role of each particular kind of atom.

Our numerical calculation of the interband part  $\varepsilon_{\alpha\beta}^{\text{abs}}(\omega)$  was performed using Eq. (4). The band energies and wave functions were calculated by the LMTO method with variational inclusion of the spin–orbit coupling.<sup>11</sup> Self-consistent spin-polarized crystal potentials were obtained using the density-functional formalism with an exchange–correlation contribution calculated according to Ref. 12. Integration in  $\mathbf{k}$  space was performed by the tetrahedron technique on the basis of 1050  $\mathbf{k}$  points in the extended Brillouin zone. The values of  $\varepsilon_{1,xx}(\omega)$  and  $\varepsilon_{2,xy}(\omega)$  were found using the Kramers–Kronig relations (2) and (3). The intraband part  $\varepsilon_{xx}(\omega)$  was calculated using Eqs. (5) and (6) and experimental values of the  $DC$  conductivity of the compounds at room temperature to evaluate the intraband collision frequency  $\gamma$ . To simulate the effects of the finite lifetime of electron excitations, we subjected  $\varepsilon_{\alpha\beta}(\omega)$  to smoothing with a width  $\Gamma(\omega) = 0.1\hbar\omega$ . The dielectric tensor thus obtained was used to calculate the frequency dependence of  $\theta_K(\omega)$  and  $\epsilon_K(\omega)$  with the aid of Eq. (1).

### 3. RESULTS OF THE CALCULATIONS OF THE MAGNETO-OPTICAL SPECTRA, THEIR ANALYSIS, AND RELATIONSHIP BETWEEN THE SPECTRA AND THE ELECTRONIC STRUCTURE OF THE COMPOUNDS

The calculated frequency dependence of  $\theta_K(\omega)$  and  $\epsilon_K(\omega)$  for PtMnSb, PdMnSb, NiMnSb, and PtMnSn is shown in Fig. 1 together with the results of the experimental investigations in Refs. 1–3. The excellent agreement between calculation and experiment for PtMnSb, especially in the vicinity of the magneto-optical resonance at  $\hbar\omega = 1.4\text{--}1.9$  eV, is noteworthy. The agreement for the other compounds is somewhat poorer. The calculation accurately reproduces the general behavior of  $\theta_K(\omega)$  and  $\epsilon_K(\omega)$  for PdMnSb and NiMnSb, but overestimates the absolute values of these quantities by a factor of 2–4 in comparison with experiment. In these compounds the extremum of  $\theta_K(\omega)$  at  $\hbar\omega \sim 1.8$  eV in the calculation is shifted 0.3–0.5 eV upward. In PtMnSn, besides the amplitude difference, there is splitting of the calculated extremum of  $\theta_K(\omega)$  at 2.5 eV, which is not observed experimentally. At the same time, the dependence of  $\epsilon_K(\omega)$  is reproduced quite satisfactorily. These differences may be due, in principle, to many-electron effects, which are not taken into account completely in the present calculation scheme. There are two more specific reasons for such differences. One is the high sensitivity of measurements of the absolute values of  $\theta_K(\omega)$  and  $\epsilon_K(\omega)$  to the state of the surface

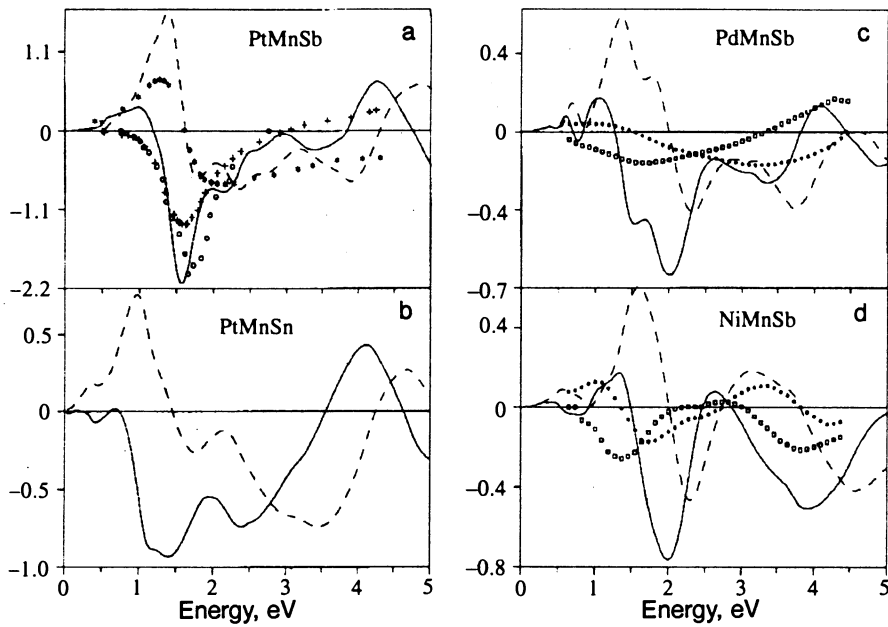


FIG. 1. Frequency dependence of the Kerr rotation  $\theta_K(\omega)$  and the Kerr ellipticity  $\epsilon_K(\omega)$  in PtMnSb (a), PtMnSn (b), PdMnSb (c), and NiMnSb (d). The solid and dashed lines are plots of the calculated values of  $\theta_K$  and  $\epsilon_K$ . Experimental data for PtMnSb: +— $\theta_K$  (Ref. 1), \*— $\epsilon_K$  (Ref. 1), o— $\theta_K$  (Ref. 3); for PdMnSb: □— $\theta_K$  (Ref. 1), \*— $\epsilon_K$  (Ref. 1); for NiMnSb: □— $\theta_K$  (Ref. 4) and \*— $\epsilon_K$  (Ref. 4).

of the samples.<sup>3</sup> A definite picture of this sensitivity is provided by a comparison of the results of the experimental investigations in Refs. 1 and 3 for PtMnSb (Fig. 1). The other possible reason is the significant influence of the intraband part of  $\epsilon_{xy}(\omega)$ , which is not taken into account in the present calculation, on the spectra of  $\theta_K(\omega)$  and  $\epsilon_K(\omega)$ . Which of these is the main reason is still unclear. However, the level of agreement between theory and experiment which has already been achieved allows us to regard the present calculations as fully realistic. In particular, they accurately describe the large extremum of  $\theta_K(\omega)$  in PtMnSb, reproduce the presence of the two energy-separated extrema of  $\theta_K(\omega)$  in NiMnSb, and correctly point out the approximately identical magnitude of the magneto-optical effects in PdMnSb, NiMnSb, and PtMnSn, which is significantly smaller than in PtMnSb. The validity of the calculation is also confirmed by a comparison of the calculated values of the optical conductivity  $\sigma_{xx}(\omega) = \omega \epsilon_{2,xx}(\omega) / 4\pi$  with the experimental results in Ref. 13 (Fig. 2). This provides some basis to study the shaping of the magneto-optical spectra of this group of compounds on the basis of the present calculations.

A comparison of our calculated off-diagonal components of the dielectric tensor  $\epsilon_{xy}(\omega) = \epsilon_{1,xy}(\omega) + i\epsilon_{2,xy}(\omega)$  (Fig. 3) with the spectra of  $\theta_K(\omega)$  shows that in PtMnSb, PdMnSb, and NiMnSb all the principal extrema of  $\theta_K(\omega)$  are directly related to corresponding extrema of  $\epsilon_{1,xy}(\omega)$ . In PtMnSn such correspondence is observed for the extremum at 1.6 eV, while the extremum of  $\theta_K(\omega)$  at  $\hbar\omega = 2.5$  eV is represented by only a small hump in the plot of  $\epsilon_{1,xy}(\omega)$ . Furthermore, in PtMnSb the principal extremum in  $\theta_K(\omega)$  is considerably stronger than the corresponding extremum in  $\epsilon_{1,xy}(\omega)$ . To verify this impression, we analyze the frequency dependence of the ratio  $\theta_K(\omega)/\epsilon_{1,xy}(\omega)$  after rewriting Eq. (1) for this purpose in the form

$$\frac{\theta_K(\omega)}{\epsilon_{1,xy}(\omega)} = \tilde{A}(\omega) + \tilde{B}(\omega) \frac{\epsilon_{2,xy}(\omega)}{\epsilon_{1,xy}(\omega)}, \quad (8)$$

where

$$\tilde{A}(\omega) = \text{Re}\{\sqrt{\epsilon_{xx}(\omega)}(1 - \epsilon_{xx}(\omega))^{-1}\},$$

$$\tilde{B}(\omega) = \text{Im}\{-[\sqrt{\epsilon_{xx}(\omega)}(1 - \epsilon_{xx}(\omega))^{-1}]\}.$$

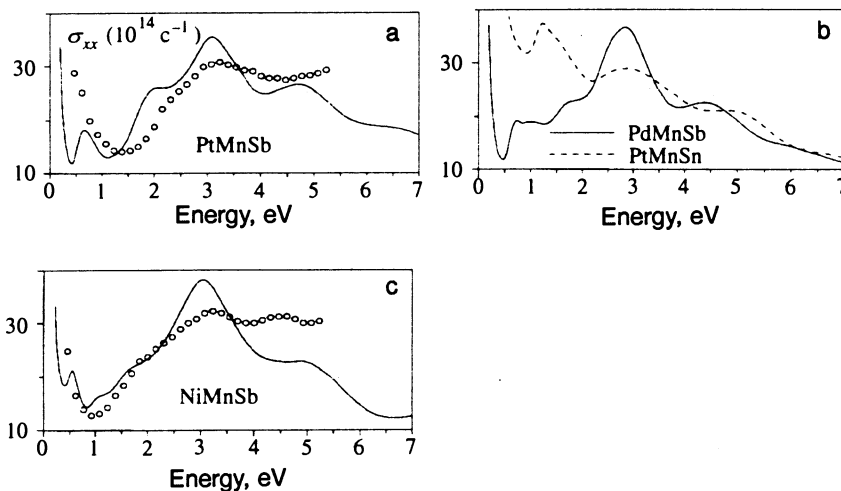


FIG. 2. Frequency dependence of the diagonal optical conductivity  $\sigma_{xx}(\omega)$  in PtMnSb, PtMnSn, PdMnSb, and NiMnSb. Solid and dashed lines—calculated values of  $\sigma_{xx}$ . Experimental data for PtMnSb (a): o— $\sigma_{xx}^{\text{exp}}(\omega)$  (Ref. 13); for NiMnSb (c): o— $\sigma_{xx}^{\text{exp}}(\omega)$  (Ref. 13).

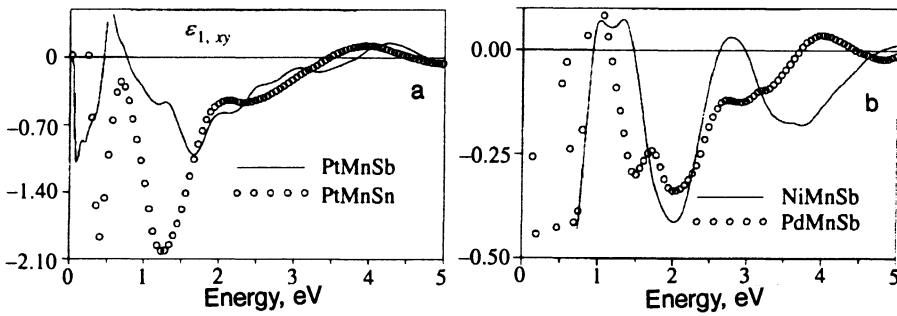


FIG. 3. Frequency dependence of the off-diagonal components of the dielectric tensor  $\varepsilon_{1,xy}(\omega)$  in PtMnSb, PtMnSn, PdMnSb, and NiMnSb.

Plots of  $\tilde{A}(\omega)$ ,  $\tilde{B}(\omega)$ , and  $\varepsilon_{2,xy}(\omega)/\varepsilon_{1,xy}(\omega)$  for PtMnSb at  $\hbar\omega=1-3$  eV are shown in Fig. 4. The plots of  $\tilde{A}(\omega)$  and  $\tilde{B}(\omega)$  have maxima in the vicinity of the minimum of  $\varepsilon_{2,xx}(\omega)$ , and the value of  $\varepsilon_{2,xy}(\omega)/\varepsilon_{1,xy}(\omega)$  at resonance is linearly dependent on the energy, as is typical of Lorentzian extrema. It is seen from Fig. 4 that the first and second terms on the right-hand side of Eq. (8) have maxima at the same frequency (energy) as  $|\varepsilon_{1,xy}(\omega)|$ . Thus, the extremum of  $\theta_K(\omega)$  is enhanced further, becoming narrower and stronger than the extremum of  $\varepsilon_{1,xy}(\omega)$ . It is noteworthy that this enhancement of the feature in  $\theta_K(\omega)$  due to the diagonal components of the dielectric tensor is observed at frequencies at which  $\varepsilon_{2,xx}(\omega) \gg |\varepsilon_{1,xx}(\omega)| \sim 1$  and the resonance condition  $\varepsilon_{1,xx}(\omega)=1$ , which was discussed in Ref. 7, is not explicitly satisfied.

The enhancement of the feature of  $\theta_K(\omega)$  in PtMnSb under consideration is due to suppression of the magneto-optical resonance in the vicinity of the local minimum of the optical conductivity, where  $\sigma_{xx}(\omega)$  is comparatively small in magnitude. In PtMnSn, where  $\sigma_{xx}(\omega)$  is significantly higher in the vicinity of the magneto-optical resonance and the conductivity minimum is shifted by almost 0.5 eV toward lower frequencies, this effect is absent. The plots of  $\tilde{A}(\omega)$ ,  $\tilde{B}(\omega)$ , and  $\varepsilon_{2,xy}(\omega)/\varepsilon_{1,xy}(\omega)$  in Fig. 5 show how the calculated value of the Kerr rotation in PtMnSn is less than half the value in PtMnSb, while the maximum of  $|\varepsilon_{1,xy}(\omega)|$  is almost twice as high. It is noteworthy that the rapid decrease in  $\sigma_{xx}(\omega)$  occurring with increasing frequency causes a strong increase in  $\tilde{A}(\omega)$  in PtMnSn. This, in turn, causes the weak feature of  $\varepsilon_{1,xy}(\omega)$  at  $\hbar\omega=2.5$  eV to grow into a second maximum of  $|\theta_K(\omega)|$  in the calculated plot of  $\theta_K(\omega)$ . Although this maximum is generally not noticeable in the experimental plot of  $\theta_K(\omega)$ , there is no reason to doubt that the small value of the Kerr rotation in PtMnSn is due exclusively to the behavior of the diagonal components of the dielectric tensor.

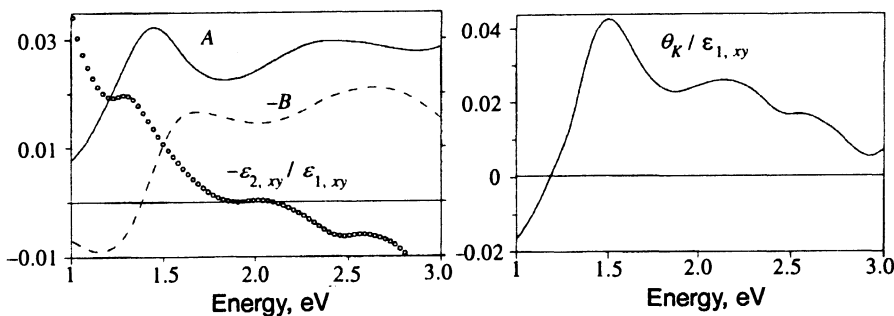


FIG. 4. Analysis of the influence of the diagonal components of the dielectric tensor on the value of the Kerr rotation in PtMnSb. For explanations see the text.

Let us now consider how the shaping of the spectra of  $\varepsilon_{1,xy}(\omega)$  in the group of compounds under consideration takes place on the microscopic level. As a first step, we dwell on the role of electron excitations with spin up and with spin down. The corresponding analysis was performed using Eq. (4), in which either the components of the wave functions with spin up or those with spin down were used to calculate the matrix elements of the momentum operator. In both of the compounds which we considered, viz., PtMnSb and PtMnSn, the electrons with spin up and the electrons with spin down make contributions of comparable magnitude. However, in PtMnSb, where the electrons with spin down have a gap at the Fermi level, only their contribution to  $\varepsilon_{1,xy}(\omega)$  exhibits resonant behavior at  $\hbar\omega=1.7$  eV (Fig. 6). The abrupt increase in optical conductivity  $\sigma_{xx}(\omega)$  at the frequency of the magneto-optical resonance is also due to the excitation of electrons with spin down, and is clearly associated with the presence of the energy gap. Thus, the half-metallic ferromagnetic state in PtMnSb provides for reconciliation between the frequency dependences of the diagonal and off-diagonal elements of the dielectric tensor, and thereby promotes an increase in the magneto-optical Kerr effect in this compound. In PtMnSn, which does not have a gap at the Fermi level, the difference between the contributions of the two spin projections is much less pronounced (Fig. 7).

To investigate the role of individual atoms in shaping the effective spin-orbit coupling, we performed a series of numerical experiments, in which the electronic structure was calculated with inclusion of the spin-orbit coupling for only one kind of atom, while  $\varepsilon_{1,xy}(\omega)$  was calculated using Eq. (4). The resulting partial contributions are presented in Fig. 8. Their sum reproduces the total value of  $\varepsilon_{1,xy}(\omega)$  to an accuracy of about 10%, as it should be according to (7). We note that in all cases, the contribution of the Mn atoms has the same characteristic frequency dependence and varies

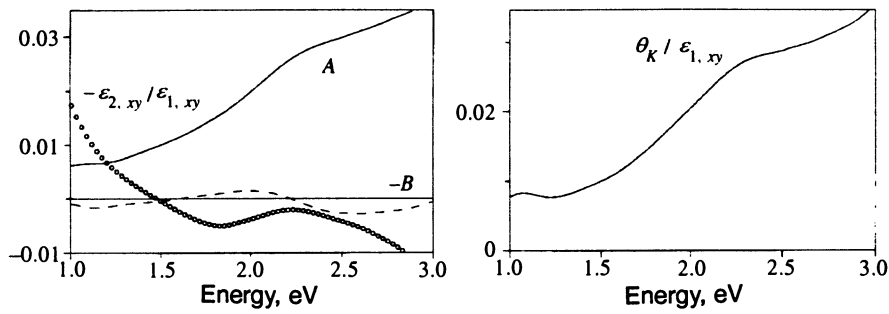


FIG. 5. Same as in Fig. 4 for PtMnSn.

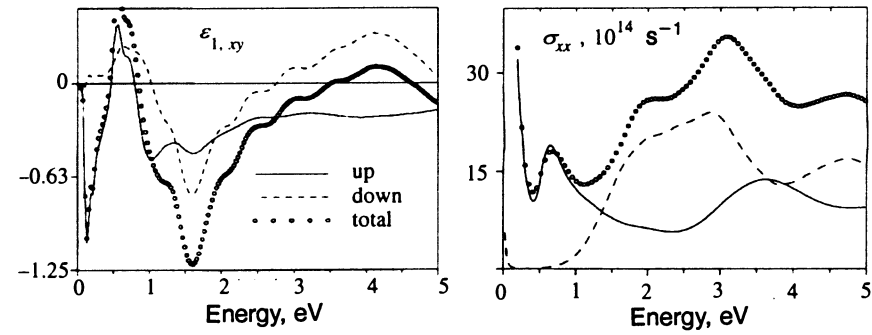


FIG. 6. Role of electrons with spin up and with spin down in shaping the spectra of  $\epsilon_{1,xy}(\omega)$  (upper half) and  $\sigma_{xx}(\omega)$  (lower half) in PtMnSb. The partial spin contributions to the total value of  $\sigma_{xx}$  are given without consideration of the intraband terms.

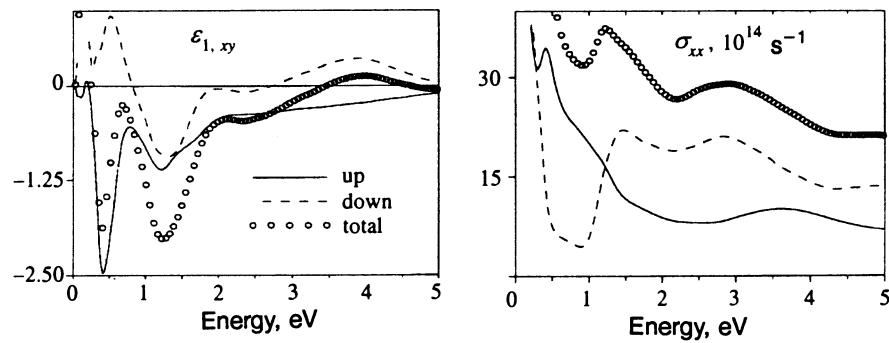


FIG. 7. Same as in Fig. 6 for PtMnSn. The partial spin contributions to the total value of  $\sigma_{xx}$  are given without consideration of the intraband terms.

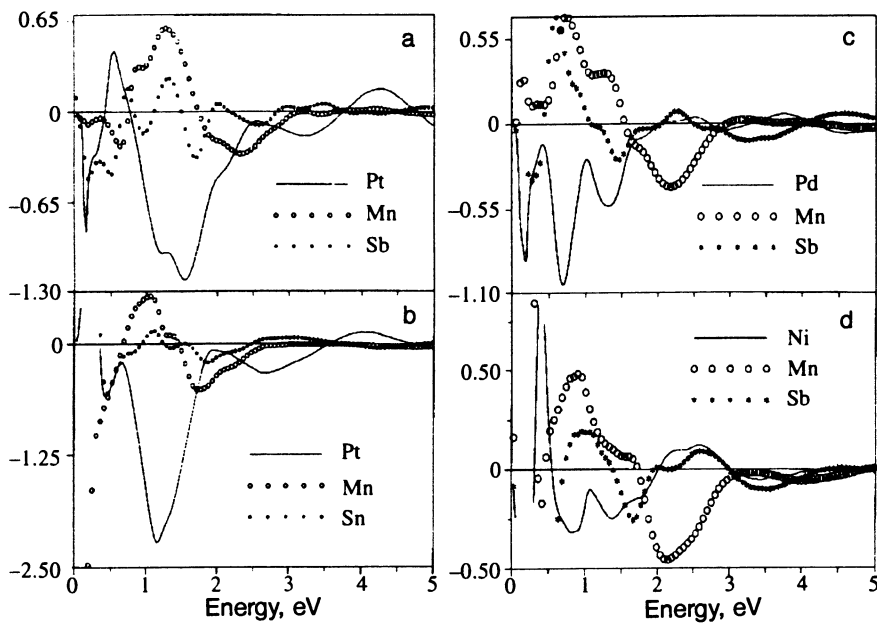


FIG. 8. Results of a numerical investigation of the effectiveness of the spin-orbit coupling in individual atoms in PtMnSb (a), PtMnSn (b), PdMnSb (c), and NiMnSb (d). For explanations see the text.

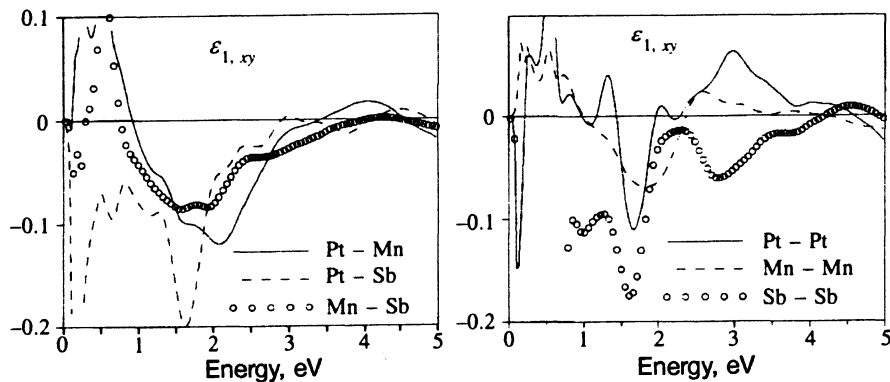


FIG. 9. Paired atomic contributions  $\varepsilon_{1,xy}^{(n,m)}(\omega)$  in PtMnSb. For explanations see the text.

only slightly from compound to compound. Similar constancy of the contributions which is associated with spin-orbit coupling, is also observed for the Sb and Pt atoms. It is attributable to the local nature of the spin-orbit coupling and can be used to qualitatively predict the behavior of  $\varepsilon_{1,xy}(\omega)$  in new materials belonging to this group of compounds. It should be stressed that the magnitude of the contribution of each kind of atom is determined not only by the nuclear charge, as in the case of the spin-orbit splitting in free atoms, but also by the spin polarization at the particular lattice site. This is manifested, in particular, by the fact that the contribution of the strongly polarized Mn atoms in all compounds considered is greater than the contribution of the Sb atoms, which have nearly twice the nuclear charge but weak spin polarization.

Let us now consider how actively the individual atoms interact with the field of the light wave, i.e., how large their contribution is to the matrix elements of the momentum operator and, through it, to  $\varepsilon_{1,xy}(\omega)$ . In order to answer this question, we conducted numerical experiments, in which the calculation of  $\varepsilon_{1,xy}(\omega)$  using Eq. (4) was performed with the matrix elements  $p_x^{i,f}(\mathbf{k})$ , which are calculated only in the atomic spheres of the  $n$ th kind of atom. The pairwise atomic contributions  $\varepsilon_{1,xy}^{(n,m)}(\omega)$  for PtMnSb are presented in Fig. 9, and those for PtMnSn are presented in Fig. 10. Since such calculations are extremely tedious, they were not performed for PdMnSb and NiMnSb. In PtMnSb our attention is attracted by the large values of the Pt-Sb and Sb-Sb contributions, which exhibit pronounced resonant behavior at  $\hbar\omega = 1.7$  eV. The Pt-Pt contribution also has a resonant character, although its magnitude is approximately half as great. The remaining contributions do not exhibit resonant behavior at the energy corresponding to the maximum of

$|\theta_k(\omega)|$ . In PtMnSn resonant behavior is exhibited by all the pairwise atomic contributions, including the Sn-Sn contributions. The Mn-Mn, Pt-Sn, and Pt-Mn contributions are the largest in magnitude. The data presented show that in PtMnSb the Pt and Sb atoms have the greatest polarizability at the resonant frequency, while in PtMnSn the resonant polarizability of all the atoms is approximately identical.

The differences noted in the off-diagonal polarizability of the atoms in PtMnSb and PtMnSn are due to differences between the electronic structures of these compounds. The partial densities of electronic states near the Fermi energy presented in Figs. 11 and 12 help us to understand their cause. In PtMnSb the Pt  $5d\uparrow$ , Mn  $3d\uparrow$ , and Sb  $5p\uparrow$  bands have fairly close energies (the corresponding positions of the band centers are  $-3.8$ ,  $-2.5$ , and  $-1.0$  eV relative to  $E_F$ ), causing strong mixing between them and, in the final analysis, the metallic type of conductivity of the bands with spin up. The picture for the bands with spin down is somewhat different. The strong exchange splitting of the Mn  $3d\downarrow$  bands causes a different relative arrangement of the band centers:  $-3.7$ ,  $+0.7$ , and  $-1.0$  eV for the Pt  $5d\downarrow$ , Mn  $3d\downarrow$ , and Sb  $5p\downarrow$  states, respectively. Comparatively strong mixing is observed here only for the Pt  $5d\downarrow$  and Sb  $5p\downarrow$  bands, while the Mn  $3d\downarrow$  band is weakly hybridized and remains fairly narrow. This is responsible for the appearance of the energy gap at the Fermi level for the electrons with spin down.<sup>2)</sup> The correspondence between the energy difference  $E(\text{Mn } 3d\downarrow) - E(\text{Sb } 5p\downarrow) = 1.7$  eV and the energy of the magneto-optical resonance is remarkable. In addition, the shape and width of the magneto-optical resonance calculated without additional smoothing are very similar to the shape and width of the narrow Mn  $3d\downarrow$  band. These data, as well as the results of the numerical experiments described above show that the

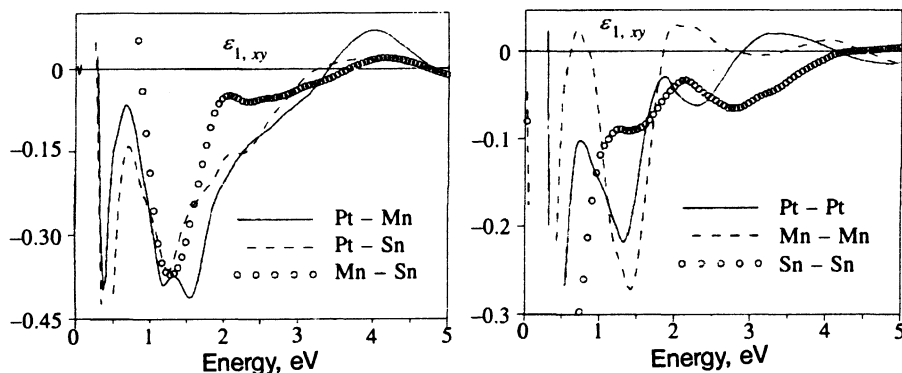


FIG. 10. Paired atomic contributions  $\varepsilon_{1,xy}^{(n,m)}(\omega)$  in PtMnSn. For explanations see the text.

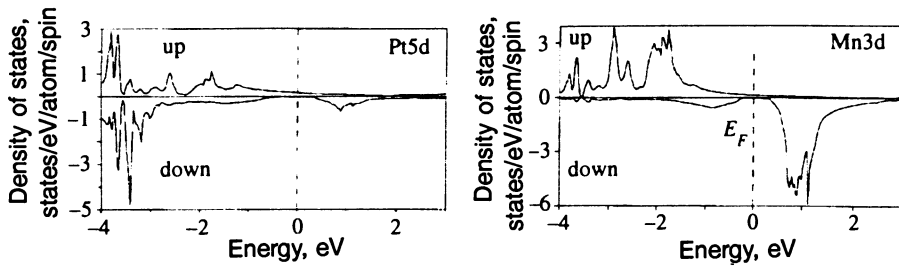
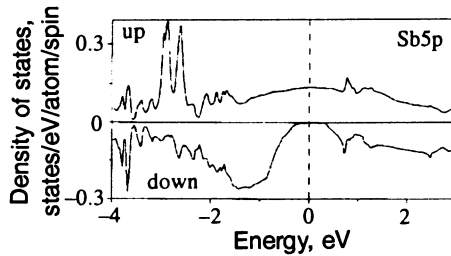


FIG. 11. Partial densities of electronic states near the Fermi level for the Pt  $5d$ , Mn  $3d$ , and Sb  $5p$  bands in PtMnSb.



magneto-optical resonance in PtMnSb forms owing to electron excitations from the hybridized  $\{\text{Pt } 5d\downarrow\text{-Sb } 5p\downarrow\}$  band to the empty Mn  $3d\downarrow$  band. These transitions occur mainly in the Pt and Sb spheres. Due to the strong hybridization of the Pt  $5d\downarrow$  and Sb  $5p\downarrow$  orbitals, the strong spin-orbit coupling at the Pt sites is also effective for the Sb sites, and the threshold for the excitation of electrons at the Pt sites is lowered to values of the order of 1.5 eV, which are characteristic of Sb sites.

In PtMnSn the density of the electronic states with spin up is approximately the same as in PtMnSb (Fig. 11). The positions of the band centers ( $-3.2$ ,  $-2.1$ , and  $+1.8$  eV for the Pt  $5d\uparrow$ , Mn  $3d\uparrow$ , and Sn  $5p\uparrow$  bands, respectively) attest to the strong hybridization of the Pt  $5d\uparrow$  and Mn  $3d\uparrow$  orbitals, which is clearly noticeable in Fig. 12. The resonant contribution of the electrons with spin up to  $\varepsilon_{1,xy}(\omega)$  is caused by electron excitations from the density-of-states peak with an energy of  $-1.4$  eV to states lying above the Fermi energy. These excitations take place, mainly, in the Pt and Mn

spheres. For the electrons with spin down, it follows from the energetic positions of the band centers  $E(\text{Pt } 5d\downarrow) = -3.2$  eV,  $E(\text{Mn } 3d\downarrow) = +1.0$  eV, and  $E(\text{Sn } 5p\downarrow) = +1.7$  eV that the Mn  $3d\downarrow$  and Sn  $5p\downarrow$  bands should be strongly hybridized. The mixed  $\{\text{Mn } 3d\downarrow\text{-Sn } 5p\downarrow\}$  band is characterized by two narrow density-of-states peaks with energies of  $-0.5$  eV and  $+1.0$  eV and a broad maximum with a center at  $+2.5$  eV. The hybridization of this set of bands with the Pt  $5d\downarrow$  states is quite moderate. The most important density-of-states peaks for magneto-optics are those with energies of  $-0.5$  eV and  $+1.0$  eV, since the transitions between them determine the resonant contribution of the electrons with spin down to  $\varepsilon_{1,xy}(\omega)$ . We note that these peaks are separated by a deep trough, which is reminiscent of the energy gap in PtMnSb. Here, however, the density of electronic states within the quasigap differs appreciably from zero, and the Fermi level is located in the upper part of the peak with the smaller energy, rather than within the gap. The result of this is the

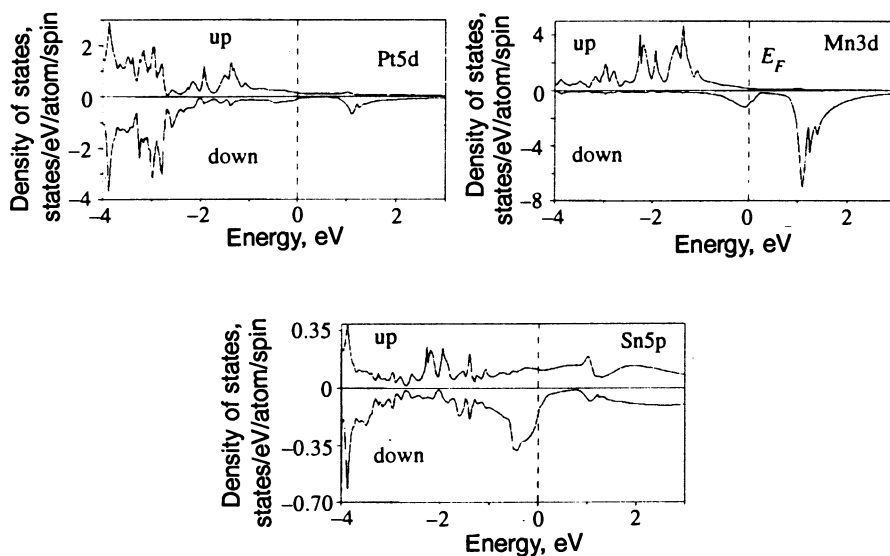


FIG. 12. Same as in Fig. 11 for PtMnSn.

metallic conductivity of the electrons with spin down in PtMnSn.

#### 4. CONCLUSIONS

The microscopic calculations of the Kerr effect in PtMnSb, PtMnSn, PdMnSb, and NiMnSb performed in the present work generally display good agreement with the experimental data. An analysis of the calculations and additional numerical experiments make it possible to reproduce the shaping of the magneto-optical spectra in this group of compounds in great detail. It offers both confirmation and refinement of previously advanced hypotheses and some new unexpected points.

In a first approximation the effect of spin-orbit scattering on an atom is a characteristic of the particular kind of atom that varies weakly from one compound to another. This observation can be useful for evaluating  $\varepsilon_{1,xy}(\omega)$  in new materials. In the present group of compounds the strongest spin-orbit coupling is associated with Pt atoms, and only their presence in the composition of the compound can provide for large values of  $\varepsilon_{1,xy}(\omega)$  and  $\theta_K(\omega)$ . The value of the matrix element of the momentum operator associated with a particular pair of atoms is more sensitive to the details of the electronic structure and the hybridization of the bands of neighboring atoms. In particular, the half-metallic ferromagnetic state realized in PtMnSb has a very significant influence on the transition matrix elements and thereby on the value of  $\varepsilon_{1,xy}(\omega)$ . Owing to the presence of a gap for electrons with spin down, the behavior of the diagonal and off-diagonal components of the dielectric tensor in this compound appears to be correlated. This results in additional enhancement of the Kerr effect accompanied by narrowing of the region of the magneto-optical resonance.

Conversely, in PtMnSn the behavior of the diagonal components promotes weakening of the Kerr effect. At the same time, the calculation indicates a maximum value of  $\varepsilon_{1,xy}(\omega)$  for the group of compounds under consideration specifically in PtMnSn. This suggests that a material with high magneto-optical activity can be obtained on the basis of

PtMnSn after appropriate adjustment of the diagonal components of the dielectric tensor either by doping or by applying thin-film coatings.

We thank G. S. Krinchik, E. S. Gan'shina, and M. M. Kirillova for some useful discussions on the subject of this work. This research was partially financed by grant No. 94-02-03680-a from the Russian Foundation for Fundamental Research.

<sup>1</sup>PdMnSb is regarded as a half-metallic ferromagnetic only in an approximation, since the Fermi level in this compound touches the top of the valence band for the electrons with spin up.

<sup>2</sup>We note that the weak hybridization of the Pt  $5d\downarrow$  and Mn  $3d\downarrow$  bands is attributable to the large difference between the positions of the band centers, while that of the Mn  $3d\downarrow$  and Sb  $5p\downarrow$  bands is attributable to the large distance between the Mn and Sb atoms in the  $C1_b$  crystal structure.

<sup>1</sup>P. G. van Engen, K. H. J. Buschow, R. Jongebreur, and M. Erman, *Appl. Phys. Lett.* **42**, 202 (1983).

<sup>2</sup>T. Inukai, N. Sugimoto, M. Matsuoka, and K. Ono, *J. Magn. Soc. Jpn.* **11**, Suppl. S1, 217 (1987).

<sup>3</sup>K. Takanashi, H. Fujimori, J. Watanabe, M. Shoji, and A. Nagai, *Jpn. J. Appl. Phys.* **27**, L2351 (1988).

<sup>4</sup>P. P. J. van Engelen, D. B. de Mooij, J. H. Wijngaard, and K. H. J. Buschow, *J. Magn. Magn. Mater.* **130**, 247 (1994).

<sup>5</sup>K. H. J. Buschow, in *Ferromagnetic Materials. A Handbook on the Properties of Magnetically Ordered Substances*, E. P. Wohlfarth and K. H. J. Buschow (eds.), North-Holland, Amsterdam (1988), Vol. 4, p. 493.

<sup>6</sup>W. Reim and J. Schoenes, *ibid.*, 1990, Vol. 5, p. 133.

<sup>7</sup>H. Feil and C. Haas, *Phys. Rev. Lett.* **58**, 65 (1987).

<sup>8</sup>R. A. de Groot, F. M. Mueller, P. G. van Engen, and K. H. J. Buschow, *Phys. Rev. Lett.* **50**, 2024 (1983).

<sup>9</sup>C. S. Wang and J. Callaway, *Phys. Rev. B* **9**, 4897 (1974); M. Singh, C. S. Wang, and J. Callaway, *Phys. Rev. B* **11**, 287 (1975); Yu. A. Uspenskii and S. V. Khalilov, *Sov. Phys. JETP* **68**, 588 (1989); H. Ebert, Habilitation Thesis, University of Munich, 1990; S. P. Lim, D. L. Price, and B. Cooper, *IEEE Trans. Magn.* **27**, 3648 (1991); P. M. Oppeneer, T. Maurer, J. Sticht, and J. Kübler, *Phys. Rev. B* **45**, 10924 (1992); K. J. Kim, T. C. Leung, B. N. Harmon, and D. W. Lynch, *J. Phys.: Condens. Matt.* **6**, 5069 (1994).

<sup>10</sup>P. N. Argyres, *Phys. Rev.* **97**, 334 (1954).

<sup>11</sup>O. K. Andersen, *Phys. Rev. B* **12**, 3060 (1975).

<sup>12</sup>U. von Barth and L. Hedin, *J. Phys. C: Solid St. Phys.* **5**, 1629 (1972).

<sup>13</sup>P. A. M. van der Heide, W. Baelde, R. A. de Groot, A. R. de Vroomen, P. G. van Engen, and K. H. J. Buschow, *J. Phys. F: Metal Phys.* **15**, L75 (1985).

Translated by P. Shelnitz